Two-Photon Interference Constructed by Two Hong–Ou–Mandel Effects in One Mach-Zehnder Interferometer *

Rui Liu(刘瑞)[1], Ling-Jun Kong(孔令军)[1], Zhou-Xiang Wang(王周祥)[1], Yu Si(司宇)[1], Wen-Rong Qi(齐文荣)[1], Shuang-Yin Huang(黄双印)[1], Chenghou Tu(涂成厚)[1], Yongnan Li(李勇男)[1]**, Hui-Tian Wang(王慧田)[2,3]**

[1]*School of Physics and Key Laboratory of Weak-Light Nonlinear Photonics, Nankai University, Tianjin 300071*
[2]*School of Physics and National Laboratory of Solid State Microstructures, Nanjing University, Nanjing 210093*
[3]*Collaborative Innovation Center of Advanced Microstructures, Nanjing 210093*

(Received 20 June 2018)

We present a two-photon interference experiment in a modified Mach-Zehnder (MZ) interferometer in which two Hong–Ou–Mandel effects occur in tandem and construct superposed two-photon states. The signal photons pass both the arms of the MZ interferometer while the idler photons pass one arm only. Interestingly, the probability of the idler photons emerging from any output port still shows a sine oscillation with the two-photon phase difference and it can be characterized only by the indistinguishability of the two-photon amplitudes. We also observe a two-photon interference pattern with a period being equal to the wavelength of the parametric photons instead of the two-photon photonic de Broglie wavelength due to the presence of two-photon phase difference, in particular, with complementary probabilities of finding the two-photon pairs in two output ports. The abundant observations can facilitate a more comprehensive understanding of the two-photon interference.

PACS: 03.65.Ud, 42.50.Dv, 42.50.Tx, 42.25.Ja DOI: 10.1088/0256-307X/35/9/090303

Two-photon interference is the most fundamental characteristic of quantum mechanics.[1,2] It takes place in a mathematical space that has no classical counterpart.[3] In other words, two-photon interference cannot be understood by the classical concepts: wave or particle. Thus it has become the real first test for an optical effect to be considered really quantum.[4] As a well-known two-photon interference experiment, the so-called Hong–Ou–Mandel (HOM) interference was firstly reported in 1987[5] and has been widely utilized as the core of many fundamental tests of quantum mechanics, such as Bell-states test,[6–8] GHZ-states test,[9,10] and quantum information including quantum key distribution,[11,12] quantum repeaters,[13,14] quantum optical coherence tomography,[15] and quantum computation.[16,17] The interference of more than two photons gives rise to more complex phenomena and may bring richer applications.[18,19] Two groups have provided independently the first experimental demonstration of genuine three-photon interference recently.[20,21] The new tools for controlling multi-photon interference may help researchers design a new toolbox of quantum optics, as the HOM effect. The HOM interference is a cancellation phenomenon of two indistinguishable output states, meaning that two 'identical' photons being simultaneously incident on the two input ports of a balanced beam splitter always emerge together from either of the output ports with a probability of 50:50. This effect has been utilized to prepare a two-photon $N00N$ state, which is useful in quantum state engineering[22,23] and photon-number path entanglement.[24,25] In particular, utilizing the multiphoton $N00N$ state and the basic Mach–Zehnder (MZ) interferometer, the photonic de Broglie wavelength can be measured[26,27] and employed to quantum metrology.[26–29] The HOM effect can be observed with not only photons but also other bosonic (quasi)particles like plasmons[30,31] and helium-4 atoms.[3] Two-photon interference always attracts researchers to study from different aspects, such as two-photon pairs independently generated from two sources[32] or temporally separated.[33]

In this Letter, we demonstrate an experiment using a modified MZ interferometer in which the two-photon pairs do not enter into the same beam splitter and meet in two different places. The superposed two-photon states are constructed by two cascaded HOM effects. Probabilities of the idler photons emerging from any output port show a sine oscillation with the path difference between the two arms, even the idler photons just pass through one arm of the MZ interferometer. This phenomenon is different from single-photon interference and can be understood by the indistinguishability of the two-photon amplitudes only. Interestingly, as is expected, we observe a two-photon interference pattern, which has a period equalling to the wavelength of the parametric photons instead of the two-photon photonic de Broglie wavelength due to the presence of two-photon phase difference. Moreover, the probabilities of finding two-photon pairs in two output ports are out of phase, which can be used to generate an $N00N$ state with tunable weight factors.

*Supported by the National Key R&D Program of China under Grant Nos 2017YFA0303800 and 2017YFA0303700, the National Natural Science Foundation of China under Grant Nos 11534006, 11774183 and 11674184, the Natural Science Foundation of Tianjin under Grant No 16JCZDJC31300, and the Collaborative Innovation Center of Extreme Optics.

**Corresponding author. Email: liyongnan@nankai.edu.cn; htwang@nju.edu.cn

© 2018 Chinese Physical Society and IOP Publishing Ltd

In the experimental setup shown in Fig. 1, a pump femtosecond (fs) laser is incident on a type-Ⅱ phase matched BBO crystal by the spontaneous parametric down-conversion (SPDC) process to generate the two-photon pairs at a degenerate wavelength of 810 nm and a repetition rate of 80 MHz. Two fiber couplers (FCs) behind narrow band-pass interference filters (IFs) are used to collect the two-photon pairs into single-mode fibers (SMFs). Two perfect single-photon Gaussian modes come out from two collimators (C1 and C2) at the end of SMFs.

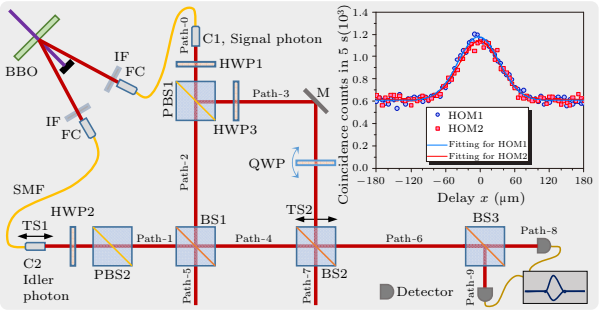

Fig. 1. Experimental setup constructed by two HOM effects in one MZ interferometer. Two-photon (signal and idler) pairs generated from the BBO crystal by the SPDC process are separately collected by FCs into SMFs and then come out from C1 and C2 in perfect Gaussian modes. IF, narrow band-pass interference filter; FC, fiber coupler; SMF, single-mode fiber; C, collimator; HWP, half wave plate; QWP, quarter-wave plate; PBS, polarization beam splitter; BS, beam splitter; M, mirror. Translation stage (TS) is used to control the delay length x. HOM1 (HOM2) effect occurs on BS1 (BS2). Two-photon state constructed by the two HOM effects is superposed in path-6 and/or path-7. Photons are collected to detectors after being separated by BS3 and make coincidence counts. Inset shows the coincidence counts of two HOM effects.

The signal photons from C1 pass through a half wave plate (HWP1) and a polarization beam splitter (PBS1). HWP1 can adjust the amount of photons transmitted to path-2 or reflected to path-3 with the aid of PBS1. The H-polarized signal photons in path-2 reach a non-polarization beam splitter (BS1), while the V-polarized signal photons in path-3 also come into the H-polarized ones after HWP3 at 45°, and then reach BS2 after being reflected by the mirror (M). After BS1, the signal photons in path-2 are reflected into path-4 with a probability of 50% and then reach BS2. The signal photons from path-3 and path-4 enter into the same path-6 (or path-7) after BS2, thus the PBS1-BS1-BS2 path and the PBS1-M-BS2 path form an MZ interferometer for the signal photons.

The H-polarized idler photons from C2 passing through HWP2 (adjusting the amount of the idler photons) and PBS2 are transmitted to path-1, and then reach to BS1 (BS2) and align well to path-4 (path-6) with the signal photons. The translation stage (TS1) controls the path difference between the idler photons in path-1 and the signal photons in path-2, thus an HOM effect (HOM1) will occur on BS1 (TS1 is fixed at the bottom of the HOM1 dip when we perform a measurement by moving TS2). Thus the bunched photon pairs are transmitted (reflected) to path-4 (path-5) with a probability of 50%.

The signal photons in path-3 and the idler photons in path-4 encounter on BS2, and another HOM effect (HOM2) occurs when the two paths are equal by moving TS2. The phase difference between two arms of the MZ interferometer is adjusted by tilting the quarter-wave plate (QWP) in path-3. To achieve the high contrast, HWP1 is rotated at a proper angle to ensure the amounts of signal photons in path-3 and path-4 are 1:1, i.e., the probabilities of the signal photons transmitted to path-2 and reflected to path-3 are 2/3 and 1/3. After BS3 separates the bunched photons into path-8 and path-9, we experimentally perform the coincidence counts between them by changing the path delay x with TS1 (TS2) to check the visibility of the HOM1 (HOM2) effect, by blocking path-3 (path-2), as shown in the inset of Fig. 1. The HOM1 (HOM2) effect shown by the blue (red) curve has a visibility of 97% (93%), meaning the alignment of the optical paths is good.

As is well known, the photon pairs produced by the SPDC process have broad spectra, especially under the fs laser pump.[34] After narrow band-pass IFs and SMFs, the input photon states coming out from C1 and C2 can be expressed as[32,33]

$$|\varphi_{\rm in}\rangle = \iint d\omega_{\rm s} d\omega_{\rm i}\, \Phi(\omega_{\rm s},\omega_{\rm i}) a_0^\dagger(\omega_{\rm s}) a_1^\dagger(\omega_{\rm i})|0\rangle, \quad (1)$$

where $\Phi(\omega_{\rm s},\omega_{\rm i})$ denotes a two-photon wave function, and $a_0^\dagger(\omega_{\rm s})$ ($a_1^\dagger(\omega_{\rm i})$) is the creation operator acting on the signal (idler) photons at a single frequency $\omega_{\rm s}$ ($\omega_{\rm i}$) in path-0 (path-1). Similarly, in the following, we use $a_j^\dagger(\omega)$ ($\omega = \omega_{\rm s}, \omega_{\rm i}$) as the creation operator in path-j ($j = 0,\ldots,9$). Due to the effects of HWP1 and PBS1, the creation operators have a relation of $a_0^\dagger(\omega_{\rm s}) = \frac{1}{\sqrt{3}}[\sqrt{2}a_2^\dagger(\omega_{\rm s}) + a_3^\dagger(\omega_{\rm s})]$. The operators of BS1 (B2, BS3) can be expressed as

$$a_u^\dagger(\omega) = \sqrt{r_{uk}}\, a_k^\dagger(\omega) + \sqrt{t_{ul}}\, a_l^\dagger(\omega), \quad (2a)$$

$$a_v^\dagger(\omega) = \sqrt{t_{vk}}\, a_k^\dagger(\omega) - \sqrt{r_{vl}}\, a_l^\dagger(\omega), \quad (2b)$$

where t_{ul} (t_{vk}) is the transmittance of the output port in path-l (path-k) from the input port in path-u (path-v), and r_{uk} (r_{vl}) is the reflectance of the output port in path-k (path-l) from the input port in path-u (path-v), respectively, and $u = 2$, $v = 1$, $k = 4$, $l = 5$ ($u = 3$, $v = 4$, $k = 6$, $l = 7$; $v = 6$, $k = 8$, $l = 9$) indicate paths of input or output ports of BS1 (BS2, BS3).

For the sake of discussion, we can let $t_{14} = r_{15} = t_{25} = r_{24} = 1/2$ for BS1 and $t_{68} = r_{69} = 1/2$ for BS3, no matter when they are signal or idler photons. Especially, as to BS2, we define $t_{37} = T'$, $r_{36} = R'$, $t_{46} = T''$, $r_{47} = R''$ when they are signal photons ($\omega = \omega_{\rm s}$), but $t_{46} = T$, $r_{47} = R$ when they are idler photons ($\omega = \omega_{\rm i}$), as shown in Fig. 2.

It is easy to conclude, $a_1^\dagger(\omega_{\rm i})|0\rangle$ has a probability of 2/3 so the HOM1 effect occurs with $a_2^\dagger(\omega_{\rm s})|0\rangle$ and

bunches together to path-4 (path-5, ignored because of futility). Then the bunched photon pairs have four possibilities to pass after BS2, as shown in Figs. 2(a)–2(d). However, the remaining $a_1^\dagger(\omega_\mathrm{i})|0\rangle$ with a probability of 1/6 does not generate the HOM1 effect and is transmitted to path-4. The HOM2 effect will occur on BS2 between the remaining idler photons $a_4^\dagger(\omega_\mathrm{i})|0\rangle$ and the signal photons $a_3^\dagger(\omega_\mathrm{s})|0\rangle$. Figures 2(e)–2(h) show the four possibilities of the photon pairs to pass after BS2.

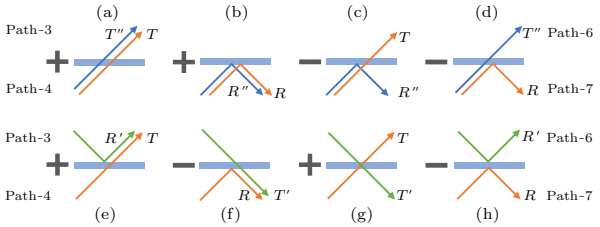

Fig. 2. All eight possibilities on BS2. The cyan (green) and orange lines represent the signal photons in path-4 (path-3) and the idler photons in path-4, respectively. The signal and idler photons are identical in all the properties. (a)–(d) The four possibilities of bunched photon pair generated from HOM1 to pass. (e)–(h) The four possibilities of HOM2. In addition, the reflection from path-4 to path-7 introduces a phase shift of π, which is required by the unitarity of the quantum evolution of BS. Possibilities, [(a) and (e), ((b) and (f)], and [(c), (d), (g) and (h)], are indistinguishable.

Thus we can construct a superposed two-photon state in path-6 and path-7 with the two cascaded HOM effects. By moving TS2, a time delay τ (length delay $x = c\tau$) in path-3 can be introduced only to signal photons, there will be abundant two-photon interference because of the indistinguishability. We use BS3 to separate the bunched photon pairs in path-6 into path-8 and/or path-9, and then make coincidence counts. The output state in path-8 and path-9 should be

$$|\varphi_{89}\rangle = \frac{-1}{2\sqrt{6}} \iint d\omega_\mathrm{s} d\omega_\mathrm{i}\, \Phi(\omega_\mathrm{s},\omega_\mathrm{i}) \sqrt{T}(\sqrt{T''} + e^{-i\omega_\mathrm{s}\tau}\sqrt{R'}) \times [a_8^\dagger(\omega_\mathrm{s}) a_9^\dagger(\omega_\mathrm{i}) + a_9^\dagger(\omega_\mathrm{s}) a_8^\dagger(\omega_\mathrm{i})]|0\rangle. \quad (3)$$

The measurement operator of the detector in path-8 or path-9 is given by

$$M_j = \int d\omega_j a_j^\dagger(\omega_j)|0\rangle\langle 0|a_j(\omega_j), \quad j = 8, 9, \quad (4)$$

where ω_j is the frequency of photons in path-j. The coincidence probability of obtaining one photon in each path is given by $P_{89} \propto \mathrm{Tr}[|\varphi_{89}\rangle\langle\varphi_{89}| M_8 \otimes M_9]$.

In general, the two-photon wave function $\Phi(\omega_\mathrm{s},\omega_\mathrm{i})$ from the SPDC process has a complex form and is inseparable, meaning that the photon pairs are frequency entanglement. However, it is not needed in our experiment, and to make the theoretical description easier, we will make a reasonable approximation. After two identical narrow band-pass IFs and SMFs, the signal and idler photons will have the same spectral characteristic and spatial mode profile. Furthermore, a high visibility of 97% of HOM1, as shown in the inset of Fig. 1, indicates that signal and idler photons coming out from C1 and C2 are both almost pure and indistinguishable.[35,36] Thus we reasonably assume that the two-photon wave function is separable, i.e., $\Phi(\omega_\mathrm{s},\omega_\mathrm{i}) = \phi(\omega_\mathrm{s})\phi(\omega_\mathrm{i})$. We assume that $\phi(\omega)$ has a normalized Gaussian profile as follows:

$$\phi(\omega) = \frac{\exp[-(\omega-\omega_0)^2/(4\sigma^2)]}{(2\pi)^{1/4}\sqrt{\sigma}}, \quad (5)$$

which is determined by the narrow band-pass IF, ω_0 is the central frequency, and $\sqrt{\sigma}$ is related to the full width at half maximum (FWHM) with FWHM$=2\sqrt{2\ln 2}\sigma$. We have the coincidence probability between path-8 and path-9 as

$$P_{89}(x) = \frac{K}{12}\Big\{2TT'' + TR'\Big[1 + \exp\Big(-\frac{\sigma^2x^2}{c^2}\Big)\Big] + 4T\sqrt{T''R'}\exp\Big(-\frac{\sigma^2x^2}{2c^2}\Big)\cos\Big(\frac{\omega_0 x}{c}\Big)\Big\}, \quad (6)$$

where K is a constant. Figure 3 shows the theoretically calculated coincidence probability of P_{89} with Eq. (6), in which the violet dots give the results when $T = T' = T'' = R = R' = R'' = 0.5$ and $K = 4$. Here we define the capital letter $P_{89}^{(\mathrm{a})-(\mathrm{h})}$ as the coincidence probability between path-8 and path-9 that is caused by the corresponding possibilities in Fig. 2(a)–2(h) (with the lower-case letter $p^{(\mathrm{a})-(\mathrm{h})}$ as the probabilities of them).

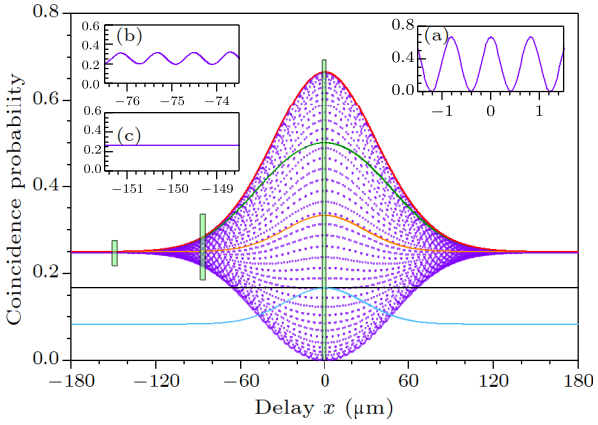

Fig. 3. Theoretically calculated coincidence probability (violet dots) of P_{89} when $T = T' = T'' = R = R' = R'' = 0.5$ and $K = 4$. The black horizontal line and sky blue curve correspond to the first and second terms in Eq. (6), and the orange curve is the sum of them. The red curve is the highest envelope of the violet dots. The green curve is the upper limit when considered in single-photon interference. Insets (a), (b), and (c) show the details of P_{89} in three delay windows of $x \in [-1.5, 1.5]$, $[-76.5, -73.5]$, and $[-151.5, -148.5]$ μm, respectively.

Firstly, we consider HOM1 or HOM2 separately, while block another. The black horizontal line in Fig. 3 corresponds to the first term in Eq. (6), indicating the coincidence counts caused by the output

state in Fig. 2(a) with a probability of $P_{89}^{(a)}(x) \equiv 1/6$ ($p^{(a)-(d)}(x) = 1/6$). It is in good agreement with the experimental result in Fig. 4, which is also a black horizontal line (only HOM1 effect). The sky blue Gaussian-profile curve in Fig. 3 corresponds to the second term in Eq. (6), indicating the coincidence counts caused by the output state in Fig. 2(e) with a probability $P_{89}^{(e)}(x)$. The probability of minimum counts is $P_{89}^{(e)}|_{x=\infty} = 1/12$ ($p^{(e)-(h)}|_{x=\infty} = 1/12$, when beyond the coherence) and the probability of maximum counts is $P_{89}^{(e)}|_{x=0} = 1/6$ ($p^{(e),(f)}|_{x=0} = 1/6$). It is also in good agreement with the experimental result shown by the sky blue Gaussian-profile curve in Fig. 4 (HOM2 effect). The orange curve in Fig. 3 is the sum of the two terms stated above, i.e., numerical superposition of HOM1 and HOM2 effects.

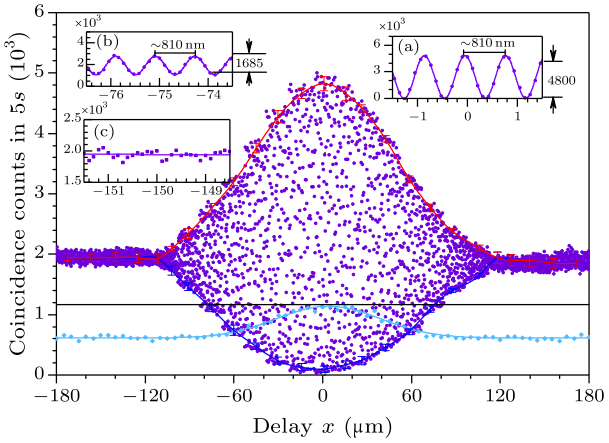

Fig. 4. Measured coincidence counts (violet dots) between path-8 and path-9 in 5 s with a delay interval of 100 nm and 3600 samples. The red and blue curves show the highest and lowest coincidence counts, respectively. The black line shows a constant coincidence when blocking path-3. The sky blue Gaussian-profile curve is the coincidence counts when blocking path-2. Insets (a), (b) and (c) show the details in three delay windows of $x \in [-1.5, 1.5]$, $[-76.5, -73.5]$, and $[-151.5, -148.5]$ μm, respectively, and the violet lines are the sine fitting curves with the same period of ~810 nm.

Secondly, we comprehensively consider the superposition state. When $x = \infty$, because of the distinguishability, numerical superposition is still valid, thus the coincidence probability is $P_{89}|_{x=\infty} = 1/4$. When $x = 0$, because of the indistinguishability, Figs. 2(g) and 2(h) are still destructive. Clearly, Figs. 2(a) and 2(e) (Figs. 2(b) and 2(f), Figs. 2(c) and 2(d)) are also indistinguishable. As a result, constructive interference occurs between Figs. 2(a) and 2(e) (Figs. 2(c) and 2(d)) as well as destructive interference between Figs. 2(b) and 2(f). After these interferences, only the Figs. 2(a), 2(c), 2(d) and 2(e) possibilities are retained with probabilities $p^{(a)}|_{x=0} = 1/3$, $p^{(c),(d)}|_{x=0} = 1/6$, and $p^{(e)}|_{x=0} = 1/3$. This implies that when $x = 0$, the bunched two-photon pairs (whether from HOM1 or HOM2) all pass to path-6 not path-7 and the coincidence probability of P_{89} is highest ($P_{89}|_{x=0} = 2/3$). In contrast, when the delay is $x = \pm\lambda/2$, the bunched two-photon pairs pass all to path-7 not path-6 and the coincidence probability is $P_{89}|_{x=\pm\lambda/2} = 0$. Thus the probabilities of finding two-photon pairs in two output ports of BS2 are out-of-phase oscillation. Differently, in an $N00N$ state interference, it is in-phase oscillation, as reported in Refs. [26,27]. Thus an $N00N$ state with weight factors can be constructed in path-6 and path-7 (output states Figs. 2(c) and 2(d) can be neglected by post-selection), and the two weight factors can be changed inversely from 0 to 1 or 1 to 0 without loss because the sum of the weight factors is a constant. To the best of our knowledge, there are no reports on the lossless adjustment for the weight factors of the $N00N$ state. On the other hand, the oscillation period is the wavelength of the parametric photons, while it is the two-photon photonic de Broglie wavelength in the traditional $N00N$ state interference as reported in Refs. [26,27]. All the properties are in good agreement with the theoretical calculation of P_{89} as shown in Fig. 3. The dependence of the upper limit of P_{89} on the delay x is shown by the red curve.

If we use only the single-photon interference to analyze the phenomenon, the signal photons no matter whether they come from path-3 or path-4 will all pass to path-6 (path-7) when $x = 0$ ($x = \pm\lambda/2$). In contrast, the idler photons have no MZ interference, thus the probabilities to path-6 and path-7 are 1 : 1. In this situation, when $x = 0$, there are four possibilities, Figs. 2(a), 2(d), 2(e) and 2(h), and every probability is double the value beyond the coherence ($p^{(a)}|_{x=0} = 1/3$, $p^{(d)}|_{x=0} = 1/3$, $p^{(e)}|_{x=0} = 1/6$ and $p^{(h)}|_{x=0} = 1/6$). Thus the coincidence probability is $P_{89}|_{x=0} = 1/2$. The green curve in Fig. 3 shows the dependence of the upper limit of P_{89} on the delay x in the situation that only the probability of signal photons emerging from any output port of BS2 oscillate. However, the red curve (indicating the real upper limit of coincidence counts) is higher than the green curve (indicating the single-photon interference), implying that the single-photon interference cannot understand this interference phenomenon. In particular, the probabilities of both signal and idler photons emerging from any output port of BS2 show a synchronous oscillation behavior. Differently from the classical interference, there are four possibilities, Figs. 2(a), 2(c), 2(d) and 2(e) when the delay $x = 0$ and the idler photons are transmitted in Figs. 2(a), 2(c) and 2(e) while reflected only in Fig. 2(d) with a ratio of 5 : 1. When $x = \pm\lambda/2$, however, the ratio between transmission and reflection becomes 1 : 5. Obviously, the probability of idler photons emerging from any output port of BS2 exhibits a sine oscillation (the theoretical ratio of maximum to minimum is 5 : 1) even without the MZ interference, because of the interferences between indistinguishable two-photon amplitudes. One should be pointed out that the two-photon interference, with an oscillation period being equal to the wavelength of degenerate parametric photons, results in the synchronous oscil-

lation of probabilities of the idler photons emerging from any output port.

In the experiment, the dependence of the coincidence counts between path-8 and path-9 on the delay x is measured by moving TS2, as shown in Fig. 4. The data graph (violet dots) is a modulated sine curve with an envelope, which has the left-right symmetry but the up-down asymmetry. The red and blue curves are the measured highest and lowest coincidence counts, respectively. In insets (a) and (b), the sine fitting curves have periods of $\Lambda_{\rm a} = \Lambda_{\rm b} \simeq 810\,{\rm nm}$, which is the same as the 810-nm wavelength of degenerate parametric photons. In inset (c), the coincidence counts are nearly a constant, thus no sine structure is exhibited. In inset (a) (or (b)), in the vicinity of $x = 0$ (or $x = 75\,\mu{\rm m}$), the coincidence counts have the highest oscillation range of ∼4800 (or ∼1685). The black horizontal line is the coincidence counts when blocking path-3 (only HOM1), and corresponds to an average counts of 1170. The sky blue Gaussian-profile curve is the coincidence counts when blocking path-2 (only HOM2) with the minimum counts of 620 and the maximum counts of 1150. The constant coincidence counts are ∼1940 when $x \to \infty$ and the maximum coincidence counts are ∼4850, corresponding to an experimental ratio of ∼2.50 with an error of 6.37% to the theoretical ratio of 8/3. Clearly, the theoretical coincidence probability of P_{89} is in good agreement with the experimental results.

In summary, we have demonstrated a two-photon interference using a modified MZ interferometer, in which two HOM effects occur in tandem and construct the superposed two-photon states. Only the signal photons pass both the arms of the MZ interferometer, while the idler photons pass one arm. Interestingly, we observe a two-photon interference with an oscillation period, which is equal to the wavelength of degenerate parametric photons, instead of the two-photon photonic de Broglie wavelength. Moreover, the probabilities of finding two-photon pairs in two output ports are out-of-phase oscillation, which is used to generate an $N00N$ state with tunable weight factors to achieve lossless adjustment. In particular, the probability of the idler photons emerging from any output port shows a sine oscillation with the path difference between two arms, even the idler photons pass only through one arm of the MZ interferometer. Such an oscillation phenomenon cannot be understood by the classical interference, whereas it originates from the indistinguishability of two-photon amplitudes. The experiment reveals that such a nonclassical phenomenon will help to deepen the understanding of two-photon interference. It should be emphasized that the HOM effect is a second-order two-photon interference, but the interference in our manuscript is a first-order two-photon interference. Our scheme may be used for quantum state engineering.

References

[1] Pan J W et al 2012 *Rev. Mod. Phys.* **84** 777
[2] Tillmann M, Tan S H, Stoeckl S E, Sanders B C, de H, Heilmann R, Nolte S, Szameit A and Walther P 2015 *Phys. Rev.* X **5** 041015
[3] Lopes R, Imanaliev A, Aspect A, Cheneau M, Boiron D and Westbrook C I 2015 *Nature* **520** 66
[4] Steel M 2014 *Nat. Photon.* **8** 273
[5] Hong C K, Ou Z Y and Mandel L 1987 *Phys. Rev. Lett.* **59** 2044
[6] Weinfurter H 1994 *Europhys. Lett.* **25** 559
[7] Mattle K, Weinfurter H, Kwiat P G and Zeilinger A 1996 *Phys. Rev. Lett.* **76** 4656
[8] Kwiat P G and Weinfurter H 1998 *Phys. Rev.* A **58** R2623
[9] Bouwmeester D, Pan J W, Daniell M, Weinfurter H and Zeilinger A 1999 *Phys. Rev. Lett.* **82** 1345
[10] Pan J W, Bouwmeester D, Daniell M, Weinfurter H and Zeilinger A 2000 *Nature* **403** 515
[11] Lo H K, Curty M and Qi B 2012 *Phys. Rev. Lett.* **108** 130503
[12] Guan J Y, Cao Z, Liu Y, Shentu G L, Pelc J S, Fejer M M, Peng C Z, Ma X, Zhang Q and Pan J W 2015 *Phys. Rev. Lett.* **114** 180502
[13] Sangouard N, Simon C, de Riedmatten H and Gisin N 2011 *Rev. Mod. Phys.* **83** 33
[14] Hofmann J, Krug M, Ortegel N, Gérard L, Weber M, Rosenfeld W and Weinfurter H 2012 *Science* **337** 72
[15] Teich M C, Saleh B E A, Wong F N C and Shapiro J H 2012 *Quantum Inf. Process.* **11** 903
[16] Kok P, Munro W J, Nemoto K, Ralph T C, Dowling J P and Milburn G J 2007 *Rev. Mod. Phys.* **79** 135
[17] Barz S, Kashefi E, Broadbent A, Fitzsimons J F, Zeilinger A and Walther P 2012 *Science* **335** 303
[18] Kwiat P G, White A G, Mitchell J R, Nairz O, Weihs G, Weinfurter H and Zeilinger A 1999 *Phys. Rev. Lett.* **83** 4725
[19] Motes K R, Olson J P, Rabeaux E J, Dowling J P, Olson S J and Rohde P P 2015 *Phys. Rev. Lett.* **114** 170802
[20] Agne S, Kauten T, Jin J, Meyer-Scott E, Salvail J Z, Hamel D R, Resch K J, Weihs G and Jennewein T 2017 *Phys. Rev. Lett.* **118** 153602
[21] Menssen A J, Jones A E, Metcalf B J, Tichy M C, Barz S, Kolthammer W S and Walmsley I A 2017 *Phys. Rev. Lett.* **118** 153603
[22] Andersen U L, Neergaard-Nielsen J S, van Loock P and Furusawa A 2015 *Nat. Phys.* **11** 713
[23] Etesse J, Bouillard M, Kanseri B and Tualle-Brouri R 2015 *Phys. Rev. Lett.* **114** 193602
[24] Kok P, Lee H and Dowling J P 2002 *Phys. Rev.* A **65** 052104
[25] Nagata T, Okamoto R, O'brien J L, Sasaki K and Takeuchi S 2007 *Science* **316** 726
[26] Edamatsu K, Shimizu R and Itoh T 2002 *Phys. Rev. Lett.* **89** 213601
[27] Walther P, Pan J W, Aspelmeyer M, Ursin R, Gasparoni S and Zeilinger A 2004 *Nature* **429** 158
[28] Mitchell M W, Lundeen J S and Steinberg A M 2004 *Nature* **429** 161
[29] Ulanov A E, Fedorov I A, Sychev D, Grangier P and Lvovsky A I 2016 *Nat. Commun.* **7** 11925
[30] Di G, Sonnefraud Y, Tame M S, Kéna-Cohen S, Dieleman F, Özdemir Ş K, Kim M S and Maier S A 2014 *Phys. Rev. Appl.* **1** 034004
[31] Fakonas J S, Lee H, Kelaita Y A and Atwater H A 2014 *Nat. Photon.* **8** 317
[32] Kim H, Lee S M and Moon H S 2015 *Sci. Rep.* **5** 9931
[33] Kim H, Lee S M and Moon H S 2016 *Sci. Rep.* **6** 34805
[34] Grice W P, Erdmann R, Walmsley I A and Branning D 1998 *Phys. Rev.* A **57** R2289
[35] Mosley P J, Lundeen J S, Smith B J, Wasylczyk P, U'Ren A B, Silberhorn C and Walmsley I A 2008 *Phys. Rev. Lett.* **100** 133601
[36] Abouraddy A F, Yarnall T M and Giuseppe G D 2013 *Phys. Rev.* A **87** 062106